Structural Premise of Selective Deubiquitinase USP30 Inhibition by Small-Molecule Benzosulfonamides

Darragh P O'Brien[1*], Hannah BL Jones[1], Franziska Guenther[2], Emma J Murphy[2], Katherine S England[2], Malcolm Anderson[3], Paul Brennan[2], John B Davis[2], Adán Pinto-Fernández[1,4], Andrew P Turnbull[5], and Benedikt M Kessler[1,3*]

[1]Target Discovery Institute, Centre for Medicines Discovery, Nuffield Department of Medicine, University of Oxford, UK

[2]ARUK-Oxford Drug Discovery Institute, Centre for Medicines Discovery, Nuffield Department of Medicine, University of Oxford, UK

[3]Waters Corporation, Wilmslow, Cheshire, UK

[4]Chinese Academy of Medical Sciences Oxford Institute, University of Oxford, UK

[5]Cancer Research Horizons, Francis Crick Institute, London, UK

*Corresponding authors: darragh.obrien@ndm.ox.ac.uk; benedikt.kessler@ndm.ox.ac.uk

Running Title:

Exploring the molecular and structural basis of USP30 inhibition

Key Words:

Mitophagy, Ubiquitin Specific Protease USP30, Benzosulfonamide, Activity-Based Protein Profiling, Enzyme Kinetics, Hydrogen Deuterium eXchange-Mass Spectrometry, Molecular Docking

ABSTRACT

Dampening functional levels of the mitochondrial deubiquitylating enzyme USP30 has been suggested as an effective therapeutic strategy against neurodegenerative disorders such as Parkinson's Disease. USP30 inhibition may counteract the deleterious effects of impaired turnover of damaged mitochondria which is inherent to both familial and sporadic forms of the disease. Small-molecule inhibitors targeting USP30 are currently in development, but little is known about their precise nature of binding to the protein. We have integrated biochemical and structural approaches to gain novel mechanistic insights into USP30 inhibition by a small-molecule benzosulfonamide containing compound, **39**. Activity-based protein profiling (ABPP) mass spectrometry confirmed target engagement, the high selectivity, and potency of **39** for USP30 against 49 other deubiquitylating enzymes in a neuroblastoma cell line. *In vitro* characterization of **39** enzyme kinetics infers slow and tight binding behavior, which is comparable with features of covalent modification of USP30. Finally, we blended hydrogen-deuterium exchange mass spectrometry and computational docking to elucidate the molecular architecture and geometry of USP30 complex formation with **39**, identifying structural rearrangements at the cleft of the USP30 thumb and palm subdomains. These studies suggest that **39** binds to the thumb-palm cleft that guides the ubiquitin C-terminus into the active site, thereby preventing ubiquitin binding and isopeptide bond cleavage, and confirming its importance in the inhibitory process. Our data will pave the way for the design and development of next-generation inhibitors targeting USP30 and associated deubiquitinylases.

INTRODUCTION

Ubiquitination is essential to protein quality control, homeostasis and lifespan.[1] Damaged proteins are flagged for removal from cells with the covalent addition of ubiquitin (Ub), a small, highly conserved 76-amino acid protein that is widely expressed across eukaryotic cell types.[2, 3] This molecular "kiss of death" proceeds through the coordinated action of E1, E2, and E3 ligase enzymes, with targeted

47 protein substrates conjugated by way of an isopeptide bond to either a single Ub molecule (mono-
48 ubiquitination), or several repeating units (poly-ubiquitination).[4] Besides the Ub-proteasome system
49 (UPS) subfamily, proteins selected for degradation can also be trafficked through the autophagy-
50 lysosome pathway. In damaged mitochondria, such autophagic clearance of impaired proteins occurs
51 through a highly selective and dedicated mechanism termed "mitophagy". Several key players work
52 tirelessly in the dysregulated mitochondrion to maintain overall cell integrity and survival, including
53 the mitochondrial outer membrane (MOM)-associated Ub serine/threonine kinase PINK1 and the
54 cytoplasmic E3 ligase Parkin.[5] PINK1 phosphorylates Ub species on damaged proteins accumulating
55 on the MOM, flagging them for elimination. This in turn recruits and activates endogenous Parkin (also
56 by phosphorylation), initiating a hyper-ubiquitination cascade that gives the green light for mitophagy
57 to proceed in a specialized autophagosome structure.[6] Deubiquitinating enzymes (DUBs) counteract
58 the actions of E3 ligases by removing Ub modifications, and several of these Ub-specific proteases
59 (USPs) have been shown to oppose Parkin activity.[7, 8] Of these, USP30 is the predominant active DUB
60 to be directly implicated in mitophagy to-date, primarily due to its localization on the MOM, whilst
61 also being linked to pexophagy and oxygen metabolism due to its widespread expression on
62 peroxisomes.[9] Interestingly, Parkin and USP30 both share an unusual preference for Lys6-linked Ub
63 chains, the mitophagic importance of which has yet to be conclusively deciphered.[10, 11]

64 Impaired mitophagy and oxidative stress have adverse roles in neurodegeneration, with both being
65 linked to familial and sporadic forms of Parkinson's Disease (PD)[12, 13]; PINK1/Parkin-mediated
66 mitophagy limits the build-up of toxic mitochondrial species in PD and loss-of-function mutations
67 occurring in the PINK1 and PRKN genes result in the progressive depletion of dopaminergic neurons
68 of the basal ganglia and a rare hereditary form of juvenile Parkinsonism.[14, 15] As USP30 antagonizes
69 mitophagy through ubiquitination, its inhibition has been proposed as a novel therapeutic strategy to
70 enhance mitochondrial turnover and clear damaged mitochondrial proteins, providing a much-needed
71 strategy to improve outcomes in PD and other neurodegenerative disorders. Several small-molecule
72 inhibitors targeting USP30 are in the pipeline, including phenylalanine derivatives, *N*-cyano

73 pyrrolidines and natural products.[16-18] Perhaps those with the greatest potential, however, are a family
74 of benzosulfonamides, most notably, compound **39**, which has been shown to boost mitophagy in
75 dopaminergic neurons of PD patients by down-regulating USP30.[19, 20] Little is currently known,
76 however, regarding the intricacies of its non-covalent attachment to USP30 itself, and the structural
77 basis of its inhibitory action. X-ray crystallography has recently provided structures of both human and
78 zebrafish USP30, but these are solely in the context of attachment to Lys6-linked di-Ub moieties.[10, 11]
79 Hydrogen/Deuterium eXchange Mass Spectrometry (HDX-MS) is a complementary biophysical tool
80 that can provide unique insights into protein structure, stability, dynamics and function.[21] In direct
81 contrast to the static snapshot provided by the crystal structure, HDX-MS monitors the conformational
82 dynamics of a system *in solution*, enabling the analysis of "proteins in motion". The technique has
83 shown particular utility for the rapid and reliable identification of small-molecule binding pockets on
84 proteins.[22] Whilst lacking the resolution of a crystal structure, the highly informative data obtained
85 from HDX-MS can be combined with orthogonal structural, computational, biochemical and/or
86 biophysical techniques to define structure activity relationships (SAR) and to direct drug discovery
87 campaigns.

88 As such, we have integrated several biophysical and structural approaches to help clarify the molecular
89 and structural interplay of **39** binding to USP30. The endogenous cellular selectivity of **39** for USP30
90 inhibition was confirmed using activity-based protein profiling mass spectrometry (ABPP-MS) against
91 a panel of 49 other endogenous DUBs in neuronal SH-SY5Y cells. Bio-layer interferometry showed that
92 **39** binds to USP30 in a slow and tight manner, which intriguingly, despite being a non-covalent binder,
93 is consistent with the profile of covalent inhibition. Finally, we combined HDX-MS and molecular
94 docking simulations to elucidate the conformational dynamics and spatial preferences of **39** binding,
95 identifying key residues in the inhibitory process itself. **39** induces conformational and structural
96 rearrangements at the cleft of the USP30 thumb and palm subdomains, in a region encompassing its
97 catalytic residues and the site of Ub binding. We postulate that these phenomena underlie the
98 mechanism of inhibition of **39**. Dampening USP30 pharmacologically may represent a tractable

99 treatment for PD and other mitophagy-related disorders. As no previous attempts to investigate the
100 molecular basis of compound **39** binding to USP30 have been reported, our data will be instrumental
101 in the development of rational next-generation inhibitors against USP30 and related DUBs.

102

103 **RESULTS AND DISCUSSION**

104 ***Compound 39 is highly potent and selective for neuronal USP30***

105 The efficacy and selectivity of compound **39** across a panel of cysteine active DUBs was initially
106 screened in SH-SY5Y neuroblastoma cell lysates by ABPP (**Figure 1a**). SH-SY5Y cell extracts were
107 treated with a range of inhibitor concentrations from 0.1 to 25 µM, followed by incubation with a HA-
108 tagged Ub-based probe with a propargylamine warhead (HA-Ub-PA). DUB probe complexes were
109 immunoprecipitated by way of their HA tag and quantified using label-free quantitation (LFQ) LC-
110 MS/MS. We implemented a data independent acquisition (DIA) MS regime to maximize the depth and
111 reproducibility of the DUB profiling assay.[23, 24] The concentration-dependent competition between
112 compound **39** and HA-Ub-PA for binding to USP30 confirmed target engagement and potency of the
113 inhibitor in a cellular matrix, with an IC_{50} value in the nanomolar range (**Figure 1b**). Moreover, **39** was
114 found to be highly selective for USP30 as it had no significant activity against any of the other 49
115 endogenous DUBs detected in the experiment (**Figure 1b**). The main cysteine-reactive DUB enzyme
116 families were all represented, with proteins containing USP, ovarian tumor protease (OTU), Ub C-
117 terminal hydrolase (UCH), and Josephin domains quantified.[25, 26] The absence of **39** concentration-
118 dependent inhibition for all other identified cysteine active DUBs demonstrates the highly selective
119 nature of the inhibitor. This selectivity is in line with previously published USP30 inhibitor selectivity
120 data from both a recombinant DUB activity panel[20] and an ABPP-MS experiment on a smaller panel of
121 endogenous DUBs identified from mouse brain tissue.[27]

122 We have recently reported that **39** can be displaced by HA-Ub-PA over long incubations.[27] Accordingly,

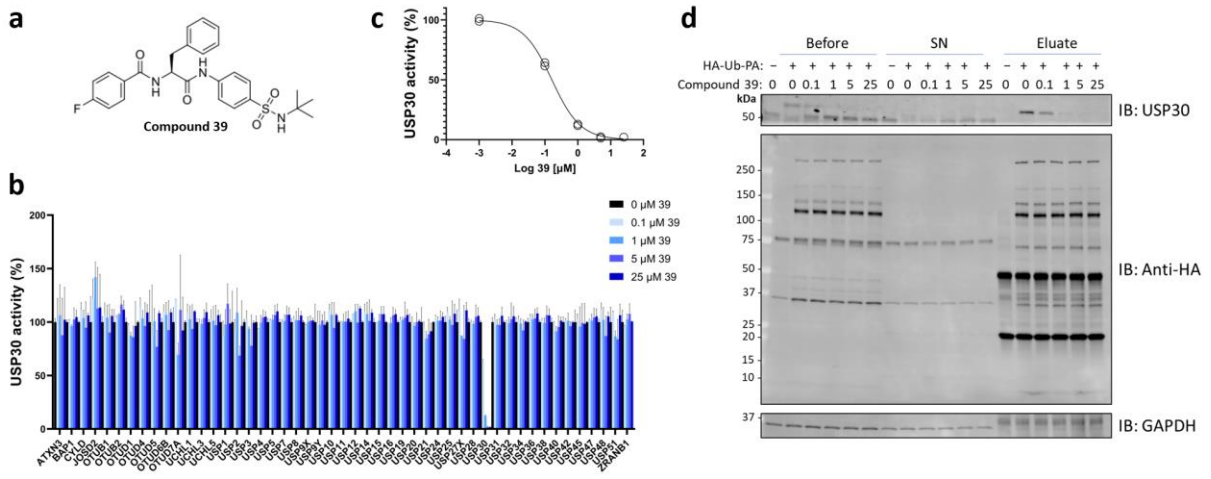

Figure 1. Compound 39 is highly potent and selective for USP30 inhibition in a cellular context. (a) Chemical structure of **39**.[27] (b) Compound **39** is a highly selective USP30 inhibitor. (c) **39** acts in a concentration dependent manner (down to 0.1 μM levels), which is in concordance with previously published data for both mouse brain and with a recombinant DUBprofiler™ (Ubiquigent) panel. (d) SHSY5Y cells were incubated with **39** for 1 h at 37˚C. The HA-Ub-PA was then incubated with **39**-treated lysates for 45 min at 37˚C at a protein ratio of 1:200 (w/w) and immunoblotted as shown. Engagement of USP30 with the probe was confirmed using anti-USP30 and anti-HA antibodies.

a small amount of displacement during the 45 min HA-Ub-PA incubation was anticipated. It is therefore expected that the IC_{50} value of 0.16 μM that we obtained from our ABPP-MS assay is likely higher than the absolute IC_{50} inhibition concentration (**Figure 1c** and **d**).

Compound 39 binds USP30 in a slow and tight manner

Once it was established that **39** down-regulates endogenous USP30 activity in a highly selective fashion, we sought to rigorously profile its inhibitory properties using a recombinant version of the protein. Synthetic full-length USP30 is very unstable and difficult to solubilize.[10] To circumvent this, we used a previously described truncated version of USP30 in our enzyme (and HDX-MS) assays, which readily went into solution and was determined to be stable over the time course of our experiments (**Figure S1**). To assess enzyme deubiquitinating efficiency, the purified USP30 construct was incubated with a fluorogenic Ub-rhodamine substrate in both the presence and absence of compound **39**. This

143 resulted in a calculated IC_{50} value for **39** of ~2 nM *in vitro*, which was in-line (albeit 10-fold lower) with
144 previous estimations (**Figure 2a**).[19] Although both measurements remain in the nM range, the 2 nM
145 IC_{50} from the Ub-rhodamine assay is lower than the 162 nM IC_{50} from the ABPP. This could be
146 attributable to differences in the endogenous and recombinant activity of USP30, non-specific
147 inhibitor occlusion in the cellular context of the ABPP, or displacement of compound 39 in the ABPP
148 by HA-Ub-PA. Progress curves for Ub-rhodamine cleaved by USP30 were used to calculate the rate of
149 inhibition. The kinetic constants k_5, k_6 and K_i gave values that were indicative of slow, tight binding
150 behavior (**Figures 2b**, **d**, **e** and **f**). The latter was visualized by a time-dependent shift of dose-response
151 inhibition curves (**Figure 2d**), as well as by plotting IC_{50} values against time (**Figure 2e**). When
152 considering the binding Scheme A (**Experimental Section**), the small value for k_6 implies that it is
153 behaving in an irreversible manner. The progress curves show typical features of an enzyme reaction
154 in the presence of a slow binding inhibitor. Furthermore, two binding events are observed in the form
155 of a) an initial and b) a steady-state velocity – both of which need to be considered during curve fitting
156 and calculation of inhibitory rates (see **Equations 2** and **3** in **Supporting Information**) (**Figure 2b**).

157 Bio-layer interferometry experiments confirmed this slow and tight binding behavior (**Figure 2c**). The
158 compound had an association rate of 0.3 $mM^{-1}s^{-1}$ and a very slow dissociation from USP30 that was
159 comparable with features of covalent modification (**Figure 2f**). This phenomenon is intriguing, as **39** is
160 known to bind to USP30 (as shown by MS), by exclusively non-covalent means.

161 ***HDX-MS kinetics identifies key residues at the compound 39 binding interface of USP30***

162 Knowledge is currently lacking on the precise location and mechanistics of **39** binding to USP30. HDX-
163 MS experiments were consequently designed to pinpoint the key regions of **39** binding to USP30,
164 whilst providing novel structural insights into the solution conformation and dynamics of complex
165 formation. HDX relies on the natural isotopic exchange of the amide backbone hydrogens of a protein
166 with deuterium when placed in a deuterated solution.[21] This leads to protein mass increases that are

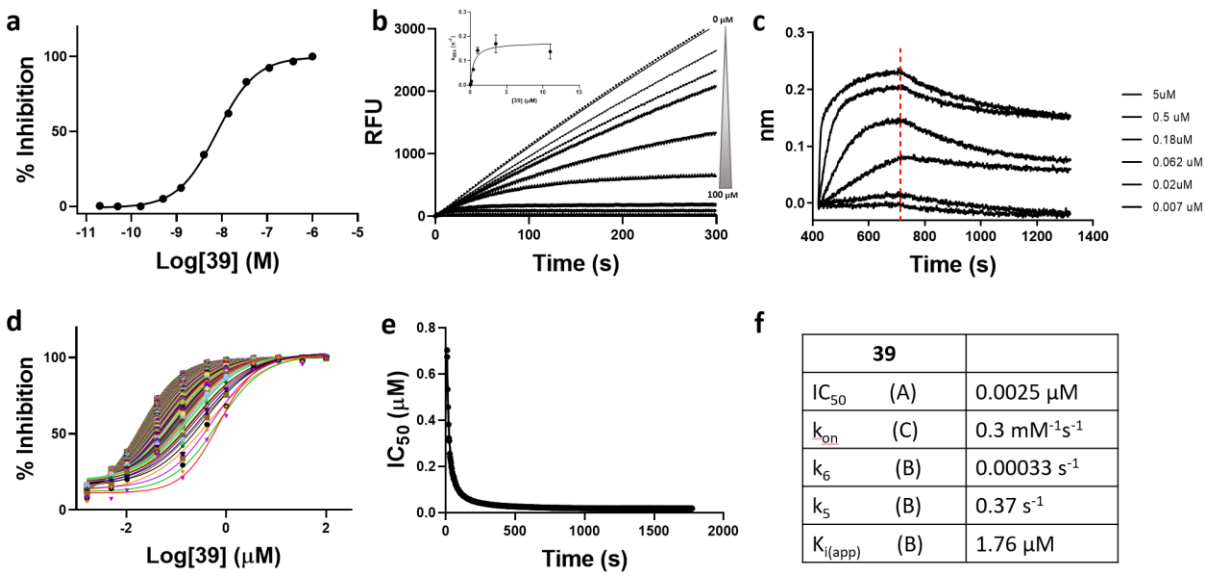

f

39		
IC_{50}	(A)	0.0025 μM
k_{on}	(C)	0.3 $mM^{-1}s^{-1}$
k_6	(B)	0.00033 s^{-1}
k_5	(B)	0.37 s^{-1}
$K_{i(app)}$	(B)	1.76 μM

Figure 2. Kinetic profiling of the non-covalent USP30 inhibitor 39. Upper panel: (a) Dose dependent inhibition of USP30 by **39**. (b) Reaction progress curves recorded on the FLIPR® Tetra. Traditional method for determining kinetic constants associated with a two-step slow, tight binding inhibitor. k_{obs}, determined by fitting the progress curves to Eq. 2 (**Supporting Information**), is plotted vs [Compound] and fitted to Eq. 3. (**Supporting Information**) to determine K_i, k_5 and k_6. (c) Bio-layer interferometry showing binding of **39** to immobilized USP30 with no detectable dissociation. Lower panel: (d) Krippendorf method[28] (**Supporting Information**) was used as an alternative way of determining kinetic constants. Time-dependent IC_{50} curves. Each curve represents inhibition data at an individual incubation time from 3-1800 sec. (e) IC_{50} values vs. incubation time fitted to Eq. 1. (**Supporting Information**) to obtain K_i and k_{inact}. As **39** is non-covalent compound but has a k_6 which is essentially 0, k_{inact} in this case represents k_5. (f) Data table of inhibition properties.

directly measurable by MS which can serve as direct probes of protein solvent accessibility and structure. Shielding of the deuterated solvent following introduction of a binding partner is indicative of a binding interface. We sought to identify such regions following **39** binding to USP30 by directly comparing the differences in HDX-MS uptake patterns of USP30 before (apo-USP30; in the presence of DMSO) and after (holo-USP30; in the presence of **39**) complex formation.

Following digestion of unlabeled USP30 with pepsin, a total of 723 peptides were generated for the protein, 133 of which were shortlisted for downstream data analysis (**Figure S2**). Selected peptides

covered 96.2% of the USP30 sequence, with an average of 4.19 peptides covering each amino acid. The kinetics of deuterium uptake was analysed for all regions of USP30, which included USP domains 1-6 and the catalytic triad at Cys77, His452 and Ser477 (**Figure S3a**). From three independent replicates, the relative fractional exchange was calculated for all peptides at each of the four time points 30, 60, 600, and 3600 sec, and plotted as a function of peptide position (**Figures 3a and S3b**).

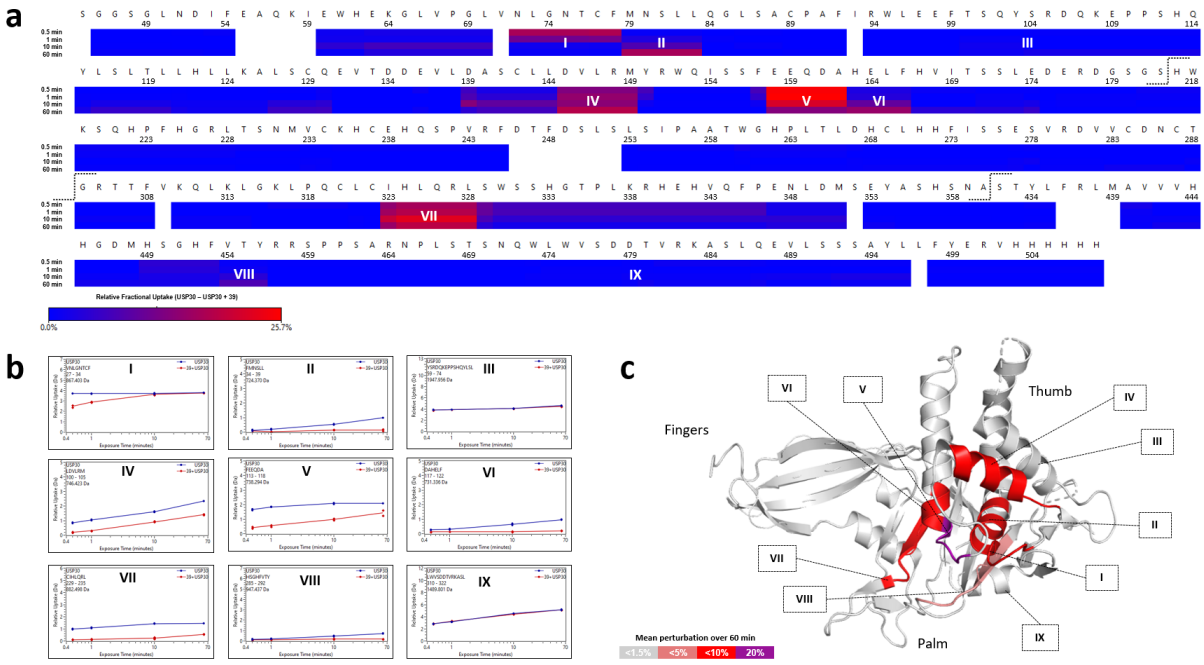

Figure 3. HDX-MS characterises the conformational dynamics of compound 39 binding to USP30. (a) Residue-level heat map indicating that compound **39** induces solvent protection in several regions of USP30. The plot displays the difference in relative fractional uptake between the holo- and apo-form of the protein over 1 h. Regions of which have the greatest perturbation following **39** binding are labeled Regions I-IX (b) Comparative uptake plots of Regions I-IX for apo- and holo-USP30 states (c) Integrated HDX-MS and X-Ray crystal structure of USP30 in complex with di-Ub. Regions of perturbation between apo- and holo-USP30 states HDX-MS data are colored according to magnitude of change. The data indicates that the **39** binding interface is located between the USP30 thumb and palm domains of the protein. Numbering is in accordance with the crystal structure of 5OHK. Dotted lines indicate the site of cleavage and removal of unstable, disordered sequences from the full-length USP30 protein.

205 Following incubation with compound **39** in conditions conducive to binary complex formation, our
206 comparative HDX-MS data indicate that the majority of USP30 is unaffected by inhibitor binding, with
207 no differences in deuterium uptake kinetics between apo- and holo-states (**Figure 3a**). This suggests
208 that **39** binding is confined to smaller subsections of the protein. Indeed, several short regions of
209 USP30 had significant shielding from the solvent in the presence of the inhibitor as compared to the
210 DMSO control, indicative of regions involved in compound binding (**Figures 3a** and **b**). The areas of
211 most significant perturbation included at two peptides spanning the USP30 catalytic Cys77 residue,
212 N72-L83 (labeled Regions I and II in **Figure 3** and highlighted in representative uptake plots in **Figure**
213 **3b**), in addition to peptides mapping to D145-M149 (Region IV), E158-F166 (Regions V and VI), I323-
214 L328 (Region VII), and finally, H449-Y456 (Region VIII), which encompasses the catalytic His452. These
215 were in direct contrast to Regions III and IX, which gave identical HDX-MS behaviors in both the apo-
216 and holo-form, reflecting the majority of the USP30 protein sequence (**Figure 3b**). The shielding
217 induced by inhibitor was greatest at the 1 h timepoint, where a difference of >25% was observed in
218 the relative fractional uptake between states. Results were confirmed by the presence of multiple
219 overlapping peptides displaying equivalent HDX-MS activity. Interestingly, no difference in
220 conformational dynamics was observed between states for the region covering the catalytic Ser477
221 (Region IX), suggesting that this site is not vital to the **39** inhibitory process, but rather, may have a
222 greater influence in determining USP30 Ub linkage preferences.[10, 11, 29] Nevertheless, targeting this site
223 to improve USP30 inhibition efficacies may prove fruitful in future design regimes.

224 No X-ray crystal structure of apo-USP30 or USP30 in complex with **39** currently exists. We therefore
225 mapped our solution HDX-MS data to PDB code 5OHK, which at a resolution of 2.34 Å, represents the
226 highest resolution 3D structure of the protein currently available in the Protein Data Bank (PDB).[10] It
227 is worth noting that this structure corresponds to USP30 in covalent complex with Lys6-linked di-Ub,
228 and as such, may give rise to subtle discrepancies when comparing across results. Nevertheless, due
229 to the lack of more suitable alternatives, we felt it a worthwhile pursuit to map our apo- and holo-
230 USP30 HDX-MS data to this 3D model. To facilitate a facile overview of the entire dataset, HDX-MS

231 results were collapsed into a single datapoint by calculating the mean perturbation between apo- and
232 holo-states across the four labeling time points. USP30 constitutes three subdomains designated
233 "thumb, palm and fingers", which is in line with related USP family members of elucidated structure.[7,
234 30] Strikingly, the shielded USP30 peptides in the presence of **39** all cluster to the same spatially
235 adjacent region of the protein, which lies at the interface of its palm and thumb subdomains (**Figure
236 3c**). Moreover, the regions with the greatest perturbation as highlighted above, I323-L328 (Region VII)
237 and H449-Y456 (Region VIII), cover areas of the protein which lie opposite each other on the 3D
238 structure. They may represent an entrance vector to the USP30 binding pocket, which is anticipated
239 to be closer to the site of greatest perturbation at E158-F166 (Regions V and VI) and the nearby
240 catalytic Cys77. The importance of these residues to the inhibitory process is further strengthened by
241 their correlation with the proposed region of USP30 binding to the Ub C-terminal tail in the crystal
242 structure.[10]

243 ***Binding of 39 alters USP30 conformation and induces rigidification in several regions***

244 Although likely to be in good agreement with the majority of 5OHK, the structural make-up of apo-
245 USP30 has yet to be experimentally confirmed. As yet, no high-resolution crystal structure exists,
246 which is of a direct consequence of the poor stability of the full-length protein itself.[10] As stated earlier,
247 a highly truncated USP30 construct was used in this study, which was devoid of its N-terminal
248 mitochondrial intermembrane domain and adjacent transmembrane domain. Furthermore, several
249 long, disordered regions were cleaved, and multiple hydrophobic residues mutated out, resulting in
250 substantially improved protein stability and solubility. As HDX-MS is not reliant on successful
251 crystallization trials, we saw this as an opportunity to describe the solution structural integrity of apo-
252 USP30, which would allow us to elucidate its mode of binding to **39**.

253 The conformational landscape of apo-USP30 generally follows the arrangement of its USP domains;
254 some of the most solvent exposed regions of the protein are found at the linker regions connecting
255 individual domains, most noticeably between USP domains 1 and 2, 4 and 5, and 5 and 6 (**Figures S3a**

256 **and S3b**). Conversely, USP domains 1 and 5 and the N-terminal end of USP domain 6 are largely
257 protected from the solvent and inaccessible (**Figure S3b**). This is in good agreement with HDX-MS data
258 recently acquired on the full length apo-USP30 protein, where the USP domains were shown to be in
259 a conformation that was generally hidden from the solvent and connected by several exposed
260 linkers.[10] However, due to the instability of the full-length species, HDX-MS was performed on a much
261 smaller scale compared to our own study, with only a sole 3 sec labeling time point measured.
262 Furthermore, an appreciation of USP30 dynamics could not be extracted from this single time point.
263 Looking at apo-USP30 dynamics across the several labeling time points described herein, an increase
264 in the rate of deuteration over the time course of the experiment was observed across the majority
265 of the protein (**Figure S3b**). This dynamic HDX-MS behavior is indicative of the presence of secondary
266 structural elements, thereby confirming the highly structured nature of the protein. The regions with
267 the greatest dynamic HDX-MS behavior were found within USP domains 2, 3, 4, and 6 (**Figure S3b**).
268 Conversely, no dynamic HDX-MS events were observed in several regions of apo-USP30 and the
269 maximum level of deuteration was reached immediately, indicating structural disorder. These
270 unstructured regions map to the N- and C-terminal extremities of the protein and within USP domains
271 1 (residues 71-78), 2 (residues 130-136), and 5 (residues 439-453). There is a high level of overlap
272 when mapping the structural data inferred from the HDX-MS to the crystal structure of 5OHK for both
273 apo- and holo-USP30 (**Figure S4**).

274 Several regions of USP30 undergo structural transitions in the presence of **39,** which are potentially
275 significant in terms of inhibitory mechanistics. First, multiple segments of USP30 become completely
276 blocked and inaccessible to the solvent following inhibitor binding. These include a region directly
277 adjacent to the catalytic Cys77 at F78-L83 and an area of USP domain 2 covering E158-F166, as
278 highlighted in purple in **Figure S4**. This suggests that **39** induces a conformation of USP30 that not only
279 blocks off the catalytic region and its surroundings from the solvent, but importantly, also prevents
280 access and binding of Ub itself. A second structural phenomenon is also evident, specifically the
281 conversion of intrinsically disordered loops in the absence of **39**, to rigid, structural elements in the

282 presence of the compound (**Figure S4**). These disorder-to-order transitions likely embody functional
283 significance[31] and in USP30, are found at the catalytic Cys77, represented by peptide V71-F78, a
284 section of USP domain 2 at R148-F154, and a long chain of residues spanning Q326-L349.

285 Tracking these structural rearrangements across individual labeling time points allows us to propose
286 a general timeline of inhibition (**Figure S5**). Taking Q326-L349 as an example, peptides mapping to this
287 region of USP30 undergo significant structural transitions at the earliest time points monitored (30
288 and 60 sec), which are completed in the later stages of our experimental time course. Conversely,
289 peptides proximal to the catalytic Cys77 become blocked and solvent inaccessible primarily in the
290 latter half of our experiment (600 and 3600 sec). The fact that the residue (and adjacent regions) most
291 crucial to USP30 catalysis, Cys77, is most significantly perturbed in the latter stages of our experiment
292 could go some way to explain the slow and tight binding behavior observed for **39** in our enzyme
293 kinetics analyses (**Figure 2**).

294 ***Molecular docking proposes key residues important for 39 binding to USP30***

295 To further refine our HDX-MS findings, we explored the binding mode of **39** to USP30 computationally.
296 We performed molecular docking simulations using the simple docking mode in AMDock software,
297 with the human USP30 catalytic domain from the crystal structure of USP30 in complex with ubiquitin
298 propargylamide (Ub-PA; PDB code = 5OHK) acting as the target receptor for the compound.[10, 19, 32] The
299 *in silico* binding pose of **39** with the highest-ranking docking score has estimated affinity and Ki values
300 of -7.9 kcal/mol and 1.62 µM respectively, compared with a reported experimental IC_{50} value of
301 approximately 20 nM.[19] Compound **39** is predicted to bind to the thumb-palm cleft that guides the Ub
302 C-terminus into the active site, residing approximately 7.4 Å away at its closest point from the thiol
303 side chain of catalytic Cys77 (**Figure 4a**). The benzyl moiety of **39** is flanked by Pro336, Met448, and
304 the side chains of Leu328 and His449 (**Figure 4b**). The fluorophenyl moiety is flanked by the side chains
305 of Leu328, Arg327, Lys338, and Tyr495, with a π-stacking interaction with His444. The N-*tert*-butyl
306 sulfonamide moiety is anchored by hydrogen-bonding interactions with the side chains of Gln326 and

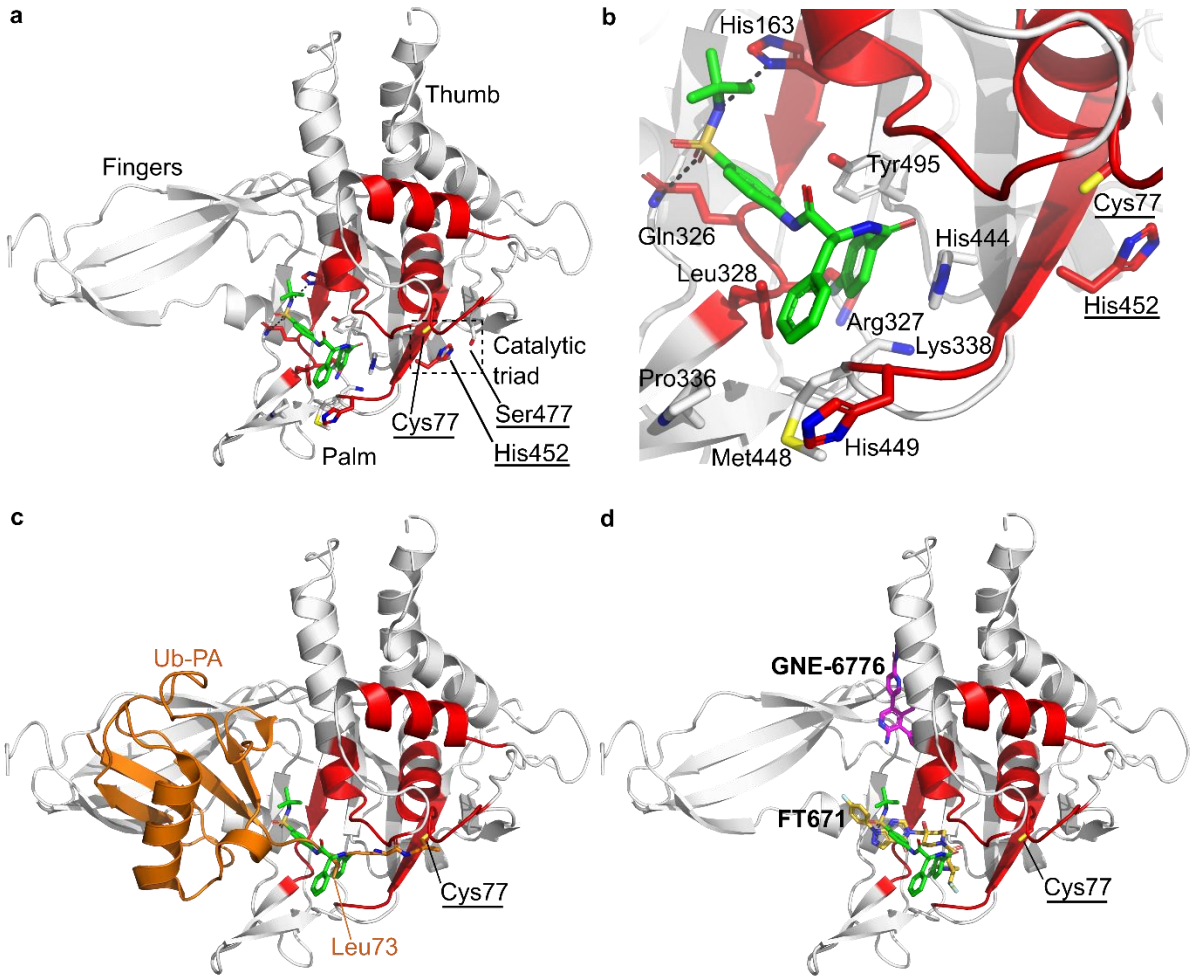

Figure 4. Modelled structure of human USP30 in complex with 39. (a) Structure of human USP30 catalytic domain highlighting the modelled position of **39** shown as a stick representation and colored green. The thumb, palm and fingers subdomains of the catalytic domain and catalytic triad (Cys77, Ser477 and His42; underlined) are highlighted. Regions identified in the HDX-MS analysis of USP30 in the presence of **39** are colored red. (b) Close-up view of the putative **39** binding site highlighting key residues and hydrogen-bonding interactions represented as dotted lines. (c) Superposition of Ub-PA (orange; PDB code= 5OHK) on the docked structure. **39** sterically clashes with the C-terminal tail of the Ub substrate thereby preventing Ub binding and isopeptide bond cleavage. (d) Superposition of the USP7 inhibitors, FT671 (yellow carbon atoms) and GNE-6776 (magenta carbon atoms) in complex with USP7, onto the docked structure. **39** putatively binds to an equivalent site in the thumb-palm cleft compared with FT671. Figure prepared using PyMOL (The PyMOL Molecular Graphics System, Version 2.4.1, Schrödinger, LLC.).

His163. Compared with the structure of USP30 in complex with Ub-PA (PDB code = 5OHK), the modelled position of **39** would sterically clash with the C-terminal tail of the Ub substrate with the

322 fluorophenyl moiety sitting in an equivalent position to the side chain of Ub Leu73, thereby preventing
323 Ub binding and isopeptide bond cleavage (**Figure 4c**).

324 Crystal structures of USP7 in complex with the small-molecule inhibitors, FT761 (PDB code= 5NGE)[30]
325 and GNE-6776 (PDB code= 5UQX)[33], reveal two distinct inhibitor binding modes that attenuate Ub
326 binding and inhibit the DUB activity. FT671 binds to the thumb-palm cleft and resides approximately
327 5 Å away from the catalytic cysteine whereas GNE-6776 interacts with acidic residues in the USP7
328 catalytic domain that mediate hydrogen-bonding interactions with the Ub Lys48 side chain and binds
329 12 Å from the catalytic cysteine. A comparison of the docked structure of **39** with the USP7 inhibitor
330 complexes suggests that **39** is most likely to bind to an equivalent site to FT671 (**Figure 4d**). In addition,
331 the docked pose of **39** correlates well with the HDX-MS data, with the predicted binding site of **39**
332 being flanked by residues residing in peptides E158-F166, I323-L328, and H449-Y456, which become
333 solvent protected in HDX-MS (**Figure 4a** and **b**). The HDX-MS analysis also implicates peptides N72-
334 L83 (which contains the catalytic Cys77) and D139-M149 in structural rearrangements upon
335 compound binding. These regions reside further from the predicted binding site of **39**. However,
336 compound binding may potentially cause conformational rearrangements of the catalytic domain
337 remote from the binding site resulting in these regions becoming protected upon compound binding.
338 Similar conformational rearrangements are seen in human USP7, in which the inhibitors bind to the
339 catalytically incompetent apoform state with switching loop "in" as compared with the catalytically
340 competent Ub-bound state with switching loop "out", and it is possible that USP30 may exhibit similar
341 dynamic conformational flexibility**.**

342

343 **CONCLUSIONS**

344 Mitochondrial pathway disruption has been linked to a spectrum of pathophysiological conditions,
345 from neurodegeneration and acute, chronic kidney and cardiovascular diseases, through to
346 hepatocellular carcinoma and peroxisome biogenesis disorders.[6, 34-36] USP30 represents an actionable

347 drug target of these conditions through its participation in PINK1/Parkin-mediated mitophagy,
348 BAX/BAK-dependent apoptosis, oncogenesis, and pexophagy.[18, 37-39] USP30 regulates mitophagy by
349 antagonizing Parkin-mediated ubiquitination and its inhibition has been shown to have significant
350 therapeutic potential against PD and similar neurodegenerative disorders. Drug discovery efforts
351 targeting USP30 have yielded the highly potent and selective small-molecule benzosulfonamide
352 inhibitor, compound **39**.[17, 19, 40] Combining state-of-the-art proteomics, HDX-MS and molecular
353 docking, we have described the dynamic structural interplay between USP30 and **39**. The inhibitor
354 binds USP30 in a slow and tight manner, and displays kinetic properties consistent with covalent
355 attachment to USP30, despite its non-covalent design. Collectively, our integrative structural biology
356 lens successfully identified regions within USP30 that undergo dramatic structural and conformational
357 rearrangements in the presence of **39**, which prevent Ub binding and decrease DUB activity. X-ray
358 data for USP30 in complex with **39** will undoubtedly complement these observations and will,
359 combined with molecular dynamics studies, drive the development of next-generation inhibitors.

360

361 **EXPERIMENTAL SECTION**

362

363 **PURITY**

364 All compounds are >95% pure by HPLC analysis (**Figure S6**).

365

366 **1. ABPP ASSAY**

367 ***HA-Ub-PA synthesis***

368 HA-Ub-PA synthesis was carried out as previously described.[27, 41] Briefly, a pTYB construct was used to
369 express Ub (Gly76del) in *E.coli*. The Ub was tagged with a HA tag on the N-terminus, and an intein-
370 chitin binding domain on the C terminus. *E.coli* lysis was performed using sonication in 50 mM Hepes,
371 150 mM NaCl, 0.5 mM Dithiothreitol (DTT). The protein was then bound to chitin bead slurry and
372 incubated with 100 mM MesNa overnight (37˚C with agitation) to form HA-Ub-MesNa. The HA-Ub-

373 MesNa was then incubated for 20 min with 250 mM propargylamine (PA; room temperature with
374 agitation), and desalted to remove excess propargylamine, resulting in the reactive activity-based
375 probe HA-Ub-PA.

376 ***Cell culture and lysis***

377 SH-SY5Y cells were cultured at 37˚C, 5% CO_2, in Eagle's Minimum Essential Medium and Ham's F12
378 Nutrient Mix (1:1), supplemented with 15% Fetal Bovine Serum, 1% non-essential amino acids and 2
379 mM Glutamax. Cells were collected by washing with phosphate-buffered saline (PBS), followed by
380 scraping in PBS and centrifugation at 200 x g. Cells were lysed in 50 mM Tris Base, 5 mM $MgCl_2.6\ H_2O$,
381 0.5 mM EDTA, 250 mM Sucrose, 1 mM DTT by vortexing with acid washed beads (1:1 v/v) 10 times (30
382 seconds vortexing, 1 min break on ice). Lysates were clarified at 600 x g for 10 min at 4˚C. Lysate
383 protein concentration was then determined by BCA.

384 ***Inhibitor selectivity with HA-Ub-PA immunoprecipitation***

385 HA-Ub-PA protein complexes were immunoprecipitated and analysed using LC-MS/MS as previously
386 described.[42] Inhibitor **39** or DMSO was incubated with 500 µg of SH-SH5Y protein lysate for 1 h at 37˚C.
387 HA-Ub-PA was then incubated with the **39**-treated lysates for 45 min at 37˚C at a protein ratio of 1:200
388 (w/w). The reaction was quenched with the addition of 0.4% SDS and 0.5% NP-40 (IGEPAL CA-630) and
389 diluted to 0.5 mg/mL with 50 mM Tris, 0.5% NP-40, 150 mM NaCl and 20 mM $MgCl_2.6\ H_2O$, pH 7.4.
390 HA-Ub-PA protein complexes were then immunoprecipitated using 150 µL of pre-washed Anti-HA
391 agarose slurry overnight at 4˚C with end-over-end rotation. The agarose slurry was then washed four
392 times and the HA-Ub-PA protein complexes were eluted using 110 µL of 2 x Laemmli buffer. To check
393 for efficient immunoprecipitation, 10 µL of the eluates were run on a western blot.

394 The remaining 100 µL of the eluates were reduced with 20 mM DTT for 10 min at 95˚C and alkylated
395 with 40 mM of iodoacetamide for 30 min at room temperature in the dark. Proteins were then
396 acidified to 1.2% phosphoric acid, diluted 6-fold with 90% methanol/100 mM TEAB, and

397 captured/washed on an S-trap column according to the standard protocol.[43] Proteins were digested
398 on the S-trap column with 2 µg of trypsin overnight at 37˚C. Eluted peptides were then dried and
399 resuspended in 2% acetonitrile (ACN), 0.1% formic acid.

400 ***LC-MS/MS***

401 Peptides were analysed using a Dionex Ultimate 3000 nano-ultra high pressure reversed-phase
402 chromatography system coupled on-line to an Orbitrap Fusion Lumos mass spectrometer (Thermo
403 Scientific). Samples were separated on an EASY-Spray PepMap RSLC C18 column (500 mm x 75 µm, 2
404 µm particle size; Thermo Scientific) over a 60 min gradient of 2-35% ACN in 5% DMSO, 0.1% formic
405 acid and at 250 nL/min. The column temperature was maintained at 50°C with the aid of a column
406 oven. The mass spectrometer was operated in positive polarity mode with a capillary temperature of
407 275°C. Data-independent acquisition (DIA) mode was utilized for automated switching between MS
408 and MS/MS acquisition as described previously.[23] Fractions were loaded with adjusted sample
409 volumes to analyze ∼200 ng on column.

410 ***DIA-MS data processing and analysis***

411 Data was analysed using DIA-NN (version 1.8) with all settings as default. A *Homo sapiens* Uniprot
412 database (retrieved on 16/04/2021) was used for the analysis. Immunoprecipitations were carried out
413 in duplicate and any DUBs that were not present in both control samples and enriched > 5-fold when
414 compared to a no probe control, were discarded from the analysis. Identifications that were assigned
415 to multiple DUBs were not included in the analysis. MINDY3 was also removed from the dataset as it
416 was the lowest intensity, so may have been at the bottom of the instruments dynamic range and did
417 not produce stable values across the dataset. All MS raw files were deposited in PRIDE under the code
418 PXD036574.

419

420 **2. ENZYME KINETICS**

421 ***In Vitro USP30 Activity Assay***

422 Fluorescence intensity measurements were used to monitor the cleavage of a Ub-rhodamine (Ub-
423 Rho110) substrate. All activity assays were performed in black 384-well plates in 20 mM Tris-HCl, pH
424 8.0, 150 mM Potassium Glutamate, 0.1 mM TCEP and 0.03% Bovine Gamma Globulin with a final assay
425 volume of 20 µL. Compound IC_{50} values for DUB inhibition were determined as previously described.[17]
426 Briefly, an 11-point dilution series of compounds were dispensed into black 384-well plates using an
427 Echo-550 Acoustic Liquid Handler (Beckman Coulter). USP30, 0.2 nM (residues 64-502Δ179-216 & 288-
428 305, Viva Biotech (Shanghai) Ltd.) was added and the plates preincubated for 30 min, 25 nM Ub-
429 Rho110 (Ubiquigent) was added to initiate the reaction and the fluorescence intensity was recorded
430 for 30 min on a Pherastar FSX (λ_{Ex} = 485 nm, λ_{Em} = 520 nm) (BMG Labtech). Initial rates were plotted
431 against compound concentration to determine IC_{50}. Data was processed using analysis tools from
432 Dotmatics (https://www.dotmatics.com/).

433 ***Kinetic assays - determination of kinetic parameters for slow-tight binding inhibitors***

434 Kinetic assays were performed in 384-well Sensoplate™ in 20 mM Tris-HCl, pH 8.0, 300 mM Potassium
435 Glutamate, 0.1 mM TCEP and 0.2% BGG with a final assay volume of 50 µL. An 11-point dilution series
436 of compound was dispensed into assay plates and 25 µL 2X Ub-Rho110 was added. The dispense
437 function of the FLIPR® Tetra (Molecular Devices) was used to add 25 µL 2X USP30 to give final assay
438 concentrations of 5 and 180 nM for USP30 and Ub-Rho110 respectively. The fluorescence signal of the
439 enzyme activity was monitored every 3 sec for 1800 sec (λ_{Ex} = 470-495 nm, λ_{Em} = 515-575 nm, camera
440 gain 70, exposure time 0.6 sec, excitation intensity 80%). Analysis was performed in GraphPad Prism
441 version 9.4.1 for Windows (Graphpad Software, La Jolla, California, USA; www.graphpad.com). The
442 time course data was normalized relative to enzyme in the absence of compound and used to generate
443 inhibition curves at each time point.

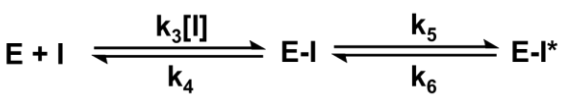

444 **Scheme A**

445 As IC_{50} values are time-dependent for compound **39** with no covalent labeling of USP30, shown by MS
446 (**Figure S1**), data were modelled to a slow-tight binding scheme (**Scheme A**). Fitting of progress curves
447 allows for calculation of relevant kinetic parameters (**Supporting Information**).

448 ***Bio-layer interferometry***

449 Bio-layer interferometry was performed on an Octet RED384® system (Sartorius) at 25°C in a buffer
450 containing 20 mM Tris-HCl (pH 8), 100 mM NaCl, 2 mM TCEP, 0.05% Tween and 1% DMSO. Biotinylated
451 USP30 (residues 64-502Δ179-216 & 288-305, Viva Biotech (Shanghai) Ltd.) was immobilized onto
452 Super Streptavidin (SSA) biosensors. After 60 sec baseline detection, the association of defined
453 concentrations of **39** (0-5 µM) was recorded over 300 sec followed by dissociation in buffer over 600
454 sec. Traces were normalised by double subtraction of baseline (no compound) and reference sensors
455 (no USP30, association and dissociation of compound) to correct for non-specific binding to the
456 sensors. Traces were analysed using the Octet Software (Version 11.2, Sartorius).

457

458 **3. HDX-MS**

459 ***HDX sample preparation***

460 USP30 was incubated in either the presence (holo-USP30) or absence (apo-USP30) of a two-fold molar
461 excess of **39**, ensuring that all complexes were fully formed and maintained over the course of the
462 labeling reaction. Before the HDX-MS experiments, labelling (L), equilibration (E) and quench (Q)
463 buffers were freshly prepared with D_2O or H_2O, respectively (Buffers E and L: 50 mM HEPES, 400 mM
464 NaCl, 2.0 mM TCEP, 10% glycerol (v/v) at pH 7.2; Buffer Q: 50 mM potassium phosphate buffer, 2.0 M
465 guanidine hydrochloride at pH 2.30). The USP30 protein sample was supplied at 66 µM and was diluted
466 in Buffer E to a final concentration of 11 µM, which equates to 16 pmol injected onto the pepsin
467 column. Buffers E and L were equilibrated at 20°C, while the protein samples and Buffer Q were
468 equilibrated at 0°C.

469 ***HDX cyclic ion mobility mass spectrometry***

470 HDX-MS experiments were carried out on a fully automated HDX-2 system (supplied by Waters,
471 Milford USA) previously described by Brown and Wilson.[44] The exchange reaction was initiated by
472 diluting 3.5 µL protein sample with a concentration of 11 µM into 56.5 µL Buffer E for reference, or
473 Buffer L for D_2O labeling, and incubated for several time points (0, 30, 60, 600 and 3600 sec). A
474 D_2O/H_2O ratio in excess of 90% guaranteed that the kinetics favored unidirectional exchange.
475 Subsequently, the exchange reaction was stopped by mixing 50 µL of sample with 50 µL pre-cooled
476 Buffer Q. Next, 50 µL of quenched sample was subjected to a temperature-controlled chromatography
477 system (HDX M-Class UPLC, Waters). The protein was digested online by a pepsin column (Enzymate
478 BEH pepsin column; 2.1 x 30 mm; Waters). Eluting peptides were trapped and washed on a C18 pre–
479 column (C18 1.7 µM VanGuard 2.1 x 5 mm pre-column; Waters) at 100 µL/min for 3 min and separated
480 on a reversed phase column (C18 1.7 µM Acquity UPLC 1 x 100 mm reverse phased column; Waters)
481 with a linear gradient ranging from 5% ACN to 40% ACN plus 0.2% FA at 40 µL/min in 8 min, followed
482 by a rapid rise to 99% ACN holding for 0.3 min. ACN concentration was rapidly reduced to 5% and held
483 there for 0.2 min, followed by a linear gradient back to 99% over 0.7 min, and holding that
484 concentration for 0.1 min. Next, C18 columns were equilibrated with 95% H_2O plus 0.2% FA for 4 min.
485 The reversed-phase chromatographic system was kept at approximately 0°C to reduce back-exchange.
486 Peptides eluting from reversed phase column were measured with a SELECT SERIES Cyclic IMS mass
487 spectrometer (Waters, Wilmslow UK) in $HDMS^E$ mode (*m/z* 50-2000). This mode utilises ion mobility
488 (IM) separation for orthogonal separation of the peptides (LC, IM, *m/z*). The mass spectrometer was
489 fitted with an electrospray source equipped with additional independent LockSpray probe (Leu-
490 enkephalin LockMass solution was used, *m/z* 556.2771).

491 ***HDX-MS data processing and analysis***

492 All MS-analyses were performed in triplicate for each time point and condition. Protein Lynx Global
493 Server (PLGS) 3.0 (Waters Corporation) was used for peptide identifications. A peptic peptide

494 sequence coverage map was generated in DynamX 3.0 HDX software (Waters Corporation). Peptide-
495 level deuterium uptake data was also visualized in DynamX (**Figure S7**) and reported as relative
496 deuterium exchange levels expressed in either mass unit or fractional exchange. The latter was
497 calculated by dividing the experimentally measured uptake by the theoretically maximum number of
498 exchangeable backbone amide hydrogens that could be replaced within each peptide. This number
499 corresponds to the number of amino acid residues present in the peptide minus the number of proline
500 residues and minus one for the N-terminus that back exchanges too rapidly to be measured by MS.[31]
501 A single charge state was considered per peptide. Data were also verified and visualized in MEMHDX.[45]

502

503 **4. MOLECULAR DOCKING**

504 The crystal structure of human USP30 catalytic domain (residues K64-V502) in covalent complex with
505 Ub-PA at 2.34 Å resolution represents the highest resolution human USP30 structure available in the
506 Protein Data Bank (PDB code= 5OHK)[10], and was used as the target receptor for docking the selective
507 USP30 benzosulfonamide inhibitor, compound **39**[19], using AutoDock Vina implemented in the program
508 AMDock 1.5.2.[32] Coordinates for **39** were generated using ChemDraw Prime 16.0.1.4, and PRODRG
509 implemented in the CCP4 software suite.[46] The compound was docked using the simple docking mode
510 and automatic defined search space in AMDock 1.5.2.

511

512 **ANCILLARY INFORMATION**

513 ***Supporting Information***

514 *This can be accessed here xxx*

515 ***PDB ID Codes***

516 *5OHK* represents the crystal structure of human USP30 catalytic domain (residues K64-V502) in
517 covalent complex with Ub propargylamide (Ub-PA) at 2.34 Å resolution. This is the highest resolution
518 structure of human USP30 currently available in the PDB.

519 ***Homology Models***

520 *Not applicable*

521 ***Corresponding Author Information***

522 *Dr Darragh P O'Brien can be contacted at darragh.obrien@ndm.ox.ac.uk*

523 *Professor Benedikt M Kessler can be contacted at benedict.kessler@ndm.ox.ac.uk*

524 ***Present/Current Author Addresses***

525 *Target Discovery Institute, Centre for Medicines Discovery, Nuffield Department of Medicine,*
526 *University of Oxford, UK* - Darragh P O'Brien, Hannah BL Jones, Benedikt M Kessler

527 *ARUK-Oxford Drug Discovery Institute, Centre for Medicines Discovery, Nuffield Department of*
528 *Medicine, University of Oxford, UK* - Franziska Guenther, Katherine S England, Emma J Murphy, Paul
529 Brennan, John B Davis

530 *Waters Corporation, Wilmslow, Cheshire, UK* - Malcolm Anderson

531 *Chinese Academy of Medical Sciences – Oxford Institute, Nuffield Department of Medicine, University*
532 *of Oxford, UK* - Adán Pinto-Fernández, Benedikt M Kessler

533 *Cancer Research Horizons, Francis Crick Institute, London, UK* - Andrew P Turnbull

534 ***Author Contributions***

535 JD and BMK designed the study. DPOB, HBLJ, FG, EM, MA, APT, and BMK wrote the first manuscript
536 draft. DPOB, HBLJ, FG, EM, MA, and APF designed and performed the experiments. APT designed and
537 performed the molecular docking. All authors discussed the results and commented on the
538 manuscript.

539 ***Acknowledgments***

540 We wish to express thanks to Drs Roman Fischer and Iolanda Vendrell from the Oxford Discovery
541 Proteomics Facility for their help with ABPP-MS data acquisition. We would like to thank Daryl S Walter
542 from Evotec and Jeff Schkeryantz from Bristol Myers Squibb for their highly useful project discussions.
543 Our gratitude goes to Alzheimer's Research UK for their support and funding for the ARUK-Oxford
544 Drug Discovery Institute (grant no. ARUK-2021DDI-OX). We would also like to thank our other funders,
545 including the Chinese Academy of Medical Sciences (CAMS) Innovation Fund for Medical Science
546 (CIFMS), China (grant number: 2018-I2M-2-002) (BMK, APF), Bayer (BMK), the late Mr & Mrs James
547 Hardwick for funding the ODDI Medicinal Chemistry Team and also the G & K Boyes Charitable Trust.

548 ***Abbreviations Used***

549 Ub, Ubiquitin; UPS, Ubiquitin Proteasome System; PD, Parkinson's Disease; MOM, Mitochondrial
550 Outer Membrane; SAR, Structure Activity Relationship; USP30, Ubiquitin Specific Protease 30; DUB,
551 Deubiquitinase; ABPP-MS, Activity-Based Protein Profiling Mass Spectrometry; LFQ, Label-Free
552 Quantitation; DIA, Data Independent Acquisition; HDX-MS, Hydrogen Deuterium eXchange Mass
553 Spectrometry; PDB, Protein Data Bank.

554

555 **REFERENCES**

556 1. Popovic, D.; Vucic, D.; Dikic, I., Ubiquitination in disease pathogenesis and treatment. *Nat*
557 *Med* **2014,** *20* (11), 1242-53.
558 2. Ciechanover, A., The ubiquitin proteolytic system and pathogenesis of human diseases: a
559 novel platform for mechanism-based drug targeting. *Biochem Soc Trans* **2003,** *31* (2), 474-81.
560 3. Pickart, C. M.; Eddins, M. J., Ubiquitin: structures, functions, mechanisms. *Biochim Biophys*
561 *Acta* **2004,** *1695* (1-3), 55-72.
562 4. Mulder, M. P.; Witting, K.; Berlin, I.; Pruneda, J. N.; Wu, K. P.; Chang, J. G.; Merkx, R.; Bialas,
563 J.; Groettrup, M.; Vertegaal, A. C.; Schulman, B. A.; Komander, D.; Neefjes, J.; El Oualid, F.; Ovaa,
564 H., A cascading activity-based probe sequentially targets E1-E2-E3 ubiquitin enzymes. *Nat Chem Biol*
565 **2016,** *12* (7), 523-30.
566 5. Pollock, L.; Jardine, J.; Urbe, S.; Clague, M. J., The PINK1 repertoire: Not just a one trick pony.
567 *Bioessays* **2021,** *43* (11), e2100168.
568 6. Bingol, B.; Sheng, M., Mechanisms of mitophagy: PINK1, Parkin, USP30 and beyond. *Free Radic*
569 *Biol Med* **2016,** *100*, 210-222.
570 7. Komander, D.; Clague, M. J.; Urbe, S., Breaking the chains: structure and function of the
571 deubiquitinases. *Nat Rev Mol Cell Biol* **2009,** *10* (8), 550-63.
572 8. Nguyen, T. N.; Padman, B. S.; Lazarou, M., Deciphering the Molecular Signals of PINK1/Parkin
573 Mitophagy. *Trends Cell Biol* **2016,** *26* (10), 733-744.
574 9. Marcassa, E.; Kallinos, A.; Jardine, J.; Rusilowicz-Jones, E. V.; Clague, M. J.; Urbe, S., New
575 aspects of USP30 biology in the regulation of pexophagy. *Autophagy* **2019,** *15* (9), 1634-1637.
576 10. Gersch, M.; Gladkova, C.; Schubert, A. F.; Michel, M. A.; Maslen, S.; Komander, D.,
577 Mechanism and regulation of the Lys6-selective deubiquitinase USP30. *Nat Struct Mol Biol* **2017,** *24*
578 (11), 920-930.
579 11. Sato, Y.; Okatsu, K.; Saeki, Y.; Yamano, K.; Matsuda, N.; Kaiho, A.; Yamagata, A.; Goto-Ito,
580 S.; Ishikawa, M.; Hashimoto, Y.; Tanaka, K.; Fukai, S., Structural basis for specific cleavage of Lys6-
581 linked polyubiquitin chains by USP30. *Nat Struct Mol Biol* **2017,** *24* (11), 911-919.
582 12. Pickrell, A. M.; Youle, R. J., The roles of PINK1, parkin, and mitochondrial fidelity in Parkinson's
583 disease. *Neuron* **2015,** *85* (2), 257-73.
584 13. Agarwal, S.; Muqit, M. M. K., PTEN-induced kinase 1 (PINK1) and Parkin: Unlocking a
585 mitochondrial quality control pathway linked to Parkinson's disease. *Curr Opin Neurobiol* **2022,** *72*,
586 111-119.
587 14. Kitada, T.; Asakawa, S.; Hattori, N.; Matsumine, H.; Yamamura, Y.; Minoshima, S.; Yokochi,
588 M.; Mizuno, Y.; Shimizu, N., Mutations in the parkin gene cause autosomal recessive juvenile
589 parkinsonism. *Nature* **1998,** *392* (6676), 605-8.
590 15. Valente, E. M.; Abou-Sleiman, P. M.; Caputo, V.; Muqit, M. M.; Harvey, K.; Gispert, S.; Ali,
591 Z.; Del Turco, D.; Bentivoglio, A. R.; Healy, D. G.; Albanese, A.; Nussbaum, R.; Gonzalez-Maldonado,
592 R.; Deller, T.; Salvi, S.; Cortelli, P.; Gilks, W. P.; Latchman, D. S.; Harvey, R. J.; Dallapiccola, B.;

Auburger, G.; Wood, N. W., Hereditary early-onset Parkinson's disease caused by mutations in PINK1. *Science* **2004,** *304* (5674), 1158-60.
16. Yue, W.; Chen, Z.; Liu, H.; Yan, C.; Chen, M.; Feng, D.; Yan, C.; Wu, H.; Du, L.; Wang, Y.; Liu, J.; Huang, X.; Xia, L.; Liu, L.; Wang, X.; Jin, H.; Wang, J.; Song, Z.; Hao, X.; Chen, Q., A small natural molecule promotes mitochondrial fusion through inhibition of the deubiquitinase USP30. *Cell Res* **2014,** *24* (4), 482-96.
17. Rusilowicz-Jones, E. V.; Jardine, J.; Kallinos, A.; Pinto-Fernandez, A.; Guenther, F.; Giurrandino, M.; Barone, F. G.; McCarron, K.; Burke, C. J.; Murad, A.; Martinez, A.; Marcassa, E.; Gersch, M.; Buckmelter, A. J.; Kayser-Bricker, K. J.; Lamoliatte, F.; Gajbhiye, A.; Davis, S.; Scott, H. C.; Murphy, E.; England, K.; Mortiboys, H.; Komander, D.; Trost, M.; Kessler, B. M.; Ioannidis, S.; Ahlijanian, M. K.; Urbe, S.; Clague, M. J., USP30 sets a trigger threshold for PINK1-PARKIN amplification of mitochondrial ubiquitylation. *Life Sci Alliance* **2020,** *3* (8).
18. Wang, F.; Gao, Y.; Zhou, L.; Chen, J.; Xie, Z.; Ye, Z.; Wang, Y., USP30: Structure, Emerging Physiological Role, and Target Inhibition. *Front Pharmacol* **2022,** *13*, 851654.
19. Kluge, A. F.; Lagu, B. R.; Maiti, P.; Jaleel, M.; Webb, M.; Malhotra, J.; Mallat, A.; Srinivas, P. A.; Thompson, J. E., Novel highly selective inhibitors of ubiquitin specific protease 30 (USP30) accelerate mitophagy. *Bioorg Med Chem Lett* **2018,** *28* (15), 2655-2659.
20. Rusilowicz-Jones, E. V.; Barone, F. G.; Lopes, F. M.; Stephen, E.; Mortiboys, H.; Urbe, S.; Clague, M. J., Benchmarking a highly selective USP30 inhibitor for enhancement of mitophagy and pexophagy. *Life Sci Alliance* **2022,** *5* (2).
21. Engen, J. R.; Wales, T. E., Analytical Aspects of Hydrogen Exchange Mass Spectrometry. *Annu Rev Anal Chem (Palo Alto Calif)* **2015,** *8*, 127-48.
22. Marciano, D. P.; Dharmarajan, V.; Griffin, P. R., HDX-MS guided drug discovery: small molecules and biopharmaceuticals. *Curr Opin Struct Biol* **2014,** *28*, 105-11.
23. Demichev, V.; Messner, C. B.; Vernardis, S. I.; Lilley, K. S.; Ralser, M., DIA-NN: neural networks and interference correction enable deep proteome coverage in high throughput. *Nat Methods* **2020,** *17* (1), 41-44.
24. Jones, H. B. L.; Heilig, R.; Davis, S.; Fischer, R.; Kessler, B. M.; Pinto-Fernandez, A., ABPP-HT*-Deep Meets Fast for Activity-Based Profiling of Deubiquitylating Enzymes Using Advanced DIA Mass Spectrometry Methods. *Int J Mol Sci* **2022,** *23* (6).
25. Komander, D., Mechanism, specificity and structure of the deubiquitinases. *Subcell Biochem* **2010,** *54*, 69-87.
26. Clague, M. J.; Urbe, S.; Komander, D., Breaking the chains: deubiquitylating enzyme specificity begets function. *Nat Rev Mol Cell Biol* **2019,** *20* (6), 338-352.
27. Jones, H. B. L.; Heilig, R.; Fischer, R.; Kessler, B. M.; Pinto-Fernandez, A., ABPP-HT - High-Throughput Activity-Based Profiling of Deubiquitylating Enzyme Inhibitors in a Cellular Context. *Front Chem* **2021,** *9*, 640105.
28. Krippendorff, B. F.; Neuhaus, R.; Lienau, P.; Reichel, A.; Huisinga, W., Mechanism-based inhibition: deriving K(I) and k(inact) directly from time-dependent IC(50) values. *J Biomol Screen* **2009,** *14* (8), 913-23.
29. Cunningham, C. N.; Baughman, J. M.; Phu, L.; Tea, J. S.; Yu, C.; Coons, M.; Kirkpatrick, D. S.; Bingol, B.; Corn, J. E., USP30 and parkin homeostatically regulate atypical ubiquitin chains on mitochondria. *Nat Cell Biol* **2015,** *17* (2), 160-9.
30. Turnbull, A. P.; Ioannidis, S.; Krajewski, W. W.; Pinto-Fernandez, A.; Heride, C.; Martin, A. C. L.; Tonkin, L. M.; Townsend, E. C.; Buker, S. M.; Lancia, D. R.; Caravella, J. A.; Toms, A. V.; Charlton, T. M.; Lahdenranta, J.; Wilker, E.; Follows, B. C.; Evans, N. J.; Stead, L.; Alli, C.; Zarayskiy, V. V.; Talbot, A. C.; Buckmelter, A. J.; Wang, M.; McKinnon, C. L.; Saab, F.; McGouran, J. F.; Century, H.; Gersch, M.; Pittman, M. S.; Marshall, C. G.; Raynham, T. M.; Simcox, M.; Stewart, L. M. D.; McLoughlin, S. B.; Escobedo, J. A.; Bair, K. W.; Dinsmore, C. J.; Hammonds, T. R.; Kim, S.; Urbe, S.; Clague, M. J.; Kessler, B. M.; Komander, D., Molecular basis of USP7 inhibition by selective small-molecule inhibitors. *Nature* **2017,** *550* (7677), 481-486.

644 31. O'Brien, D. P.; Durand, D.; Voegele, A.; Hourdel, V.; Davi, M.; Chamot-Rooke, J.; Vachette,
645 P.; Brier, S.; Ladant, D.; Chenal, A., Calmodulin fishing with a structurally disordered bait triggers CyaA
646 catalysis. *PLoS Biol* **2017,** *15* (12), e2004486.
647 32. Valdes-Tresanco, M. S.; Valdes-Tresanco, M. E.; Valiente, P. A.; Moreno, E., AMDock: a
648 versatile graphical tool for assisting molecular docking with Autodock Vina and Autodock4. *Biol Direct*
649 **2020,** *15* (1), 12.
650 33. Kategaya, L.; Di Lello, P.; Rouge, L.; Pastor, R.; Clark, K. R.; Drummond, J.; Kleinheinz, T.;
651 Lin, E.; Upton, J. P.; Prakash, S.; Heideker, J.; McCleland, M.; Ritorto, M. S.; Alessi, D. R.; Trost, M.;
652 Bainbridge, T. W.; Kwok, M. C. M.; Ma, T. P.; Stiffler, Z.; Brasher, B.; Tang, Y.; Jaishankar, P.; Hearn,
653 B. R.; Renslo, A. R.; Arkin, M. R.; Cohen, F.; Yu, K.; Peale, F.; Gnad, F.; Chang, M. T.; Klijn, C.;
654 Blackwood, E.; Martin, S. E.; Forrest, W. F.; Ernst, J. A.; Ndubaku, C.; Wang, X.; Beresini, M. H.; Tsui,
655 V.; Schwerdtfeger, C.; Blake, R. A.; Murray, J.; Maurer, T.; Wertz, I. E., USP7 small-molecule inhibitors
656 interfere with ubiquitin binding. *Nature* **2017,** *550* (7677), 534-538.
657 34. Honsho, M.; Okumoto, K.; Tamura, S.; Fujiki, Y., Peroxisome Biogenesis Disorders. *Adv Exp*
658 *Med Biol* **2020,** *1299*, 45-54.
659 35. Schmidt, M. F.; Gan, Z. Y.; Komander, D.; Dewson, G., Ubiquitin signalling in
660 neurodegeneration: mechanisms and therapeutic opportunities. *Cell Death Differ* **2021,** *28* (2), 570-
661 590.
662 36. Pan, W.; Wang, Y.; Bai, X.; Yin, Y.; Dai, L.; Zhou, H.; Wu, Q.; Wang, Y., Deubiquitinating
663 enzyme USP30 negatively regulates mitophagy and accelerates myocardial cell senescence through
664 antagonism of Parkin. *Cell Death Discov* **2021,** *7* (1), 187.
665 37. Bingol, B.; Tea, J. S.; Phu, L.; Reichelt, M.; Bakalarski, C. E.; Song, Q.; Foreman, O.;
666 Kirkpatrick, D. S.; Sheng, M., The mitochondrial deubiquitinase USP30 opposes parkin-mediated
667 mitophagy. *Nature* **2014,** *510* (7505), 370-5.
668 38. Liang, J. R.; Martinez, A.; Lane, J. D.; Mayor, U.; Clague, M. J.; Urbe, S., USP30 deubiquitylates
669 mitochondrial Parkin substrates and restricts apoptotic cell death. *EMBO Rep* **2015,** *16* (5), 618-27.
670 39. Riccio, V.; Demers, N.; Hua, R.; Vissa, M.; Cheng, D. T.; Strilchuk, A. W.; Wang, Y.;
671 McQuibban, G. A.; Kim, P. K., Deubiquitinating enzyme USP30 maintains basal peroxisome abundance
672 by regulating pexophagy. *J Cell Biol* **2019,** *218* (3), 798-807.
673 40. Harrigan, J. A.; Jacq, X.; Martin, N. M.; Jackson, S. P., Deubiquitylating enzymes and drug
674 discovery: emerging opportunities. *Nat Rev Drug Discov* **2018,** *17* (1), 57-78.
675 41. Borodovsky, A.; Ovaa, H.; Kolli, N.; Gan-Erdene, T.; Wilkinson, K. D.; Ploegh, H. L.; Kessler,
676 B. M., Chemistry-based functional proteomics reveals novel members of the deubiquitinating enzyme
677 family. *Chem Biol* **2002,** *9* (10), 1149-59.
678 42. Pinto-Fernandez, A.; Davis, S.; Schofield, A. B.; Scott, H. C.; Zhang, P.; Salah, E.; Mathea, S.;
679 Charles, P. D.; Damianou, A.; Bond, G.; Fischer, R.; Kessler, B. M., Comprehensive Landscape of Active
680 Deubiquitinating Enzymes Profiled by Advanced Chemoproteomics. *Front Chem* **2019,** *7*, 592.
681 43. HaileMariam, M.; Eguez, R. V.; Singh, H.; Bekele, S.; Ameni, G.; Pieper, R.; Yu, Y., S-Trap, an
682 Ultrafast Sample-Preparation Approach for Shotgun Proteomics. *J Proteome Res* **2018,** *17* (9), 2917-
683 2924.
684 44. Brown, K. A.; Wilson, D. J., Bottom-up hydrogen deuterium exchange mass spectrometry: data
685 analysis and interpretation. *Analyst* **2017,** *142* (16), 2874-2886.
686 45. Hourdel, V.; Volant, S.; O'Brien, D. P.; Chenal, A.; Chamot-Rooke, J.; Dillies, M. A.; Brier, S.,
687 MEMHDX: an interactive tool to expedite the statistical validation and visualization of large HDX-MS
688 datasets. *Bioinformatics* **2016,** *32* (22), 3413-3419.
689 46. Winn, M. D.; Ballard, C. C.; Cowtan, K. D.; Dodson, E. J.; Emsley, P.; Evans, P. R.; Keegan, R.
690 M.; Krissinel, E. B.; Leslie, A. G.; McCoy, A.; McNicholas, S. J.; Murshudov, G. N.; Pannu, N. S.;
691 Potterton, E. A.; Powell, H. R.; Read, R. J.; Vagin, A.; Wilson, K. S., Overview of the CCP4 suite and
692 current developments. *Acta Crystallogr D Biol Crystallogr* **2011,** *67* (Pt 4), 235-42.

693